Available online at www.sciencedirect.com
ScienceDirect
Proceedings of the Combustion Institute 31 (2007) 2029–2036
Proceedings of the Combustion Institute
www.elsevier.com/locate/proci

Combustion of nano-aluminum and liquid water ☆

G.A. Risha [a,*], S.F. Son [b], R.A. Yetter [a], V. Yang [a], B.C. Tappan [b]

[a] The Pennsylvania State University, University Park, PA 16870, USA
[b] Los Alamos National Laboratory, Los Alamos, NM, USA

Abstract

An experimental investigation on the combustion behavior of nano-aluminum (nAl) and liquid water has been conducted. In particular, linear and mass-burning rates of quasi-homogeneous mixtures of nAl and liquid water as a function of pressure, mixture composition, particle size, and oxide layer thickness were measured. This study is the first reported self-deflagration on nAl and liquid water without the use of any additional gelling agent. Steady-state burning rates were obtained at room temperature (~25 °C) using a windowed vessel for a pressure range of 0.1–4.2 MPa in an argon atmosphere, particle diameters of 38–130 nm, and overall mixture equivalence ratios (ϕ) from 0.5 to 1.25. At the highest pressure studied, the linear burning rate was found to be 8.6 ± 0.4 cm/s, corresponding to a mass-burning rate per unit area of 6.1 g/cm^2 s. The pressure exponent at room temperature was 0.47, which was independent of the overall mixture equivalence ratio for all of the cases considered. The mass-burning rate per unit area increased from ~1.0 to 5.8 g/cm^2 s for an equivalence ratio range of 0.5–1.25. It varied inversely to particle diameter, increasing by 157% when the particle diameter was decreased from 130 to 50 nm at $\phi = 1.0$.

Keywords: Aluminum; Water; Combustion; Burning rate; Nano-aluminum

1. Introduction

The aluminum–water reaction is important to many combustion and explosive systems. When aluminum burns in a composite solid propellant, the Al typically reacts with combustion products of the energetic oxidizer and binder, such as H_2O and CO_2 [1–3]. The combustion of Al with seawater is of interest to underwater propulsion, since the reaction is extremely exothermic and the water (oxidizer) need not be carried onboard [4]. Such reaction has also been proposed as a method to produce hydrogen for high-speed air breathing propulsion (e.g., by carrying and reacting *in situ* an Al/H_2O mixture vs. carrying cryogenic hydrogen and the associated delivery system) [5]. In addition, the Al/H_2O reaction has been studied in reference to nuclear reactor safety [6] and underwater explosives.

The combustion of Al with water is fundamentally an interesting system, because without preheat, the reaction is predicted to occur as a heterogeneous process in contrast to a vaporization process followed by a gas-phase reaction as typically occurs when aluminum reacts in air [7–11]. Figure 1 shows the adiabatic flame temperatures of stoichiometric Al/air and Al/liquid water along with the Al vaporization temperature as a function of pressure. As seen from the figure, except at atmospheric pressure and slightly higher, the flame temperature of the Al/liquid water reac-

☆ Supplementary data for this article can be accessed online. See Appendix A.

* Corresponding author. Fax: +1 814 949 5190.
E-mail address: gar108@psu.edu (G.A. Risha).

1540-7489/$ - see front matter © 2006 The Combustion Institute. Published by Elsevier Inc. All rights reserved.
doi:10.1016/j.proci.2006.08.056

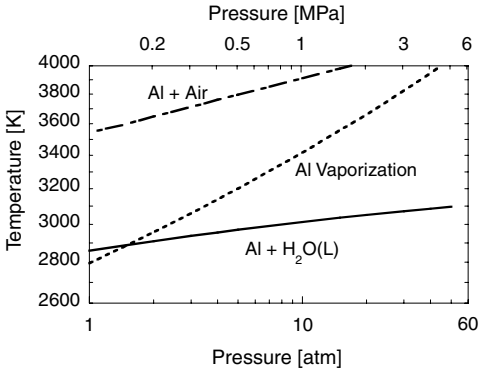

Fig. 1. Adiabatic flame temperatures of aluminum combustion in stoichiometric mixtures of air and liquid water.

tion is lower than the vaporization temperature of Al, suggesting that combustion must initially proceed through a surface reaction like boron and carbon. However, unlike boron and carbon, the final oxide product, if formed or present on the particle surface, will not leave the surface since its vaporization temperature is considerably higher than both the Al vaporization and adiabatic flame temperatures. Experimentally, this change in combustion mode has been qualitatively observed for the combustion of single micron-sized particles in steam at atmospheric pressure [7] and in air as pressure is increased from 1 to 60 atm [12].

The use of nano-sized particles in the aluminum–water reaction can offer significant advantages over larger size particles. Much of the highly desirable traits of nano-sized metal powders in combustion systems can be attributed to their high specific surface area (high reactivity) and overall small dimensions (short reaction times). Nano-sized aluminum (nAl) has also been shown to have lower ignition temperatures [13–15] than micron-sized particles, which are closer to the melting temperature of aluminum (~973 K) vs. the melting temperature of the passivating oxide shell (~2327 K). Because of their small size and high surface area, they are natural gelling agents in liquid particle systems. Considerable uncertainty remains in the understanding of how nAl particles burn. Due to their size, kinetic control may be anticipated vs. diffusion control. However, if condensed-phase processes are important, the reaction may remain diffusion controlled as predicted by a shrinking core model where the fuel and oxidizer need to diffuse through a liquid or solid oxide layer [16].

Few fundamental combustion studies have been conducted on nAl in pure water environments. Parr et al. [13] have studied ignition temperatures and burning times of nAl in low concentrations of postcombustion gases of stoichiometric $H_2/O_2/Ar$ flames. Particularly relevant to the present study is the work of Ivanov [17,18], who investigated the effect of pressure on ultrafine aluminum metal powders (UFP) in a mixture of liquid water in the presence of a thickening agent, polyacrylamide (3%). The nano-sized particles of their study were formed by the exploding-wire technique and generally are agglomerates with sizes ranging from 10s to 100s of nanometers. The stoichiometric and fuel-lean ($\phi = 0.67$) mixtures studied had high mass loadings of Al (e.g., much higher than the gas-phase studies of Parr et al. [13]), but would not ignite without including the polyacrylamide thickening agent in the mixture.

In the present research, we further investigate the Al–liquid H_2O reaction with nano-sized particles, which are smaller in size, spherical in shape, and have controlled oxide layers. The results show that a gelling agent was not required with the smaller spherical particles and that much higher burning rates were achieved. The effects of pressure, mixture ratio, particle size, and oxide layer thickness on the burning characteristics are examined. The results are important to attain a better understanding of the combustion processes of nAl particles and the resulting flame structure of a simple two-component heterogeneous system. The fundamentals learned from this system can then be applied to other more complex nanoenergetic systems such as metastable intermolecular composite systems (MICs) [19–21], where the oxidizer is a solid metal oxide, generally in a particulate form just as the metal (e.g., nAl and MoO_3).

2. Experiment

The burning rates of nAl–H_2O mixtures were obtained using a constant volume optical pressure vessel under well-controlled operating conditions in an argon environment, as shown schematically in Fig. 2. The chamber, constructed from 316 stainless steel, is equipped with four optical

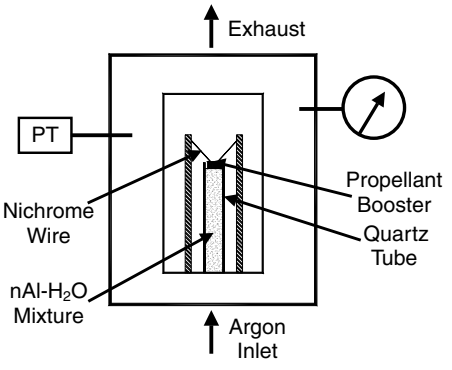

Fig. 2. Schematic diagram of windowed pressure vessel.

viewing ports each having a 15.2×2.54 cm field of view. The 61-cm long chamber has an inner diameter of 22 cm and a total free volume of 23 L to minimize the pressure variation caused by the generation of gaseous combustion products during an experiment. The base plate has six feedthrough ports to provide pathways into the chamber for electrical-signal and gas lines. One of the optical viewing ports was backlit through an optical diffuser, which evenly distributes the light emitted from the light source located outside the test chamber. The opposite viewing port of the diffuser was used for real-time recording of the burning process by a digital video camera.

The nAl particles used in the present study were supplied from Technanogy and Nanotechnologies and ranged in sizes from 38 to 130 nm in diameter (Table 1). The active aluminum content varied from approximately 54–84% by mass. Particle densities, inclusive of the oxide coating, were measured using a pycnometer and had values near 3 g/cm^3 (as compared to bulk Al of 2.7 g/cm^3). The particles from Nanotechnologies were specifically selected to investigate the effects of particle size effects with the same oxide-layer thickness of ~2 nm and the effects of oxide thickness for a specific particle diameter of ~80 nm. It should be noted that the actual diameters of the specified 80-nm particles are 71 ± 7 and 70 nm, respectively, according to the small angle scattering (SAS) and Brunauer, Emmett, and Teller (BET) particle characterization measurements performed by Mang (personal communication with Dr. Joseph T. Mang of Los Alamos National Laboratory, November 2005). Figure 3 shows a scanning electron microscope (SEM) micrograph of the 80-nm aluminum particles showing the particles are highly spherical.

The nAl particles were mixed in small batches with distilled water in a sealed plastic bag. Stoichiometry was calculated was based upon the active aluminum content in the particle. The mixture was then loaded into a quartz tube with a 10 mm OD (8 mm ID) $\times$ 75 mm length. A small ignition booster made of a homogeneous, double-base gun propellant (NOSOL 363) was placed atop the strand. The packing density of each sample was calculated by measuring the fill length and mass contained in the quartz tube. A Mettler balance with a resolution of 10^{-2} milligram was used to measure the sample mass. The sample was loaded in the pressure vessel immediately after packing to avoid any loss through vaporization or slow, low temperature reactions. Packing densities of the samples ranged from 0.71 to 1.48 g/cm^3 with standard deviations of 0.016–0.106 g/cm^3 (Table 2). For the 38-nm diameter particles, a higher equivalence ratio was found to have a lower packing density. As the overall equivalence ratio approaches infinity (i.e., no water in mixture), the maximum packing density was found to be 0.35 g/cm^3. Conversely, as the overall equivalence ratio approached zero, the packing density becomes that of water.

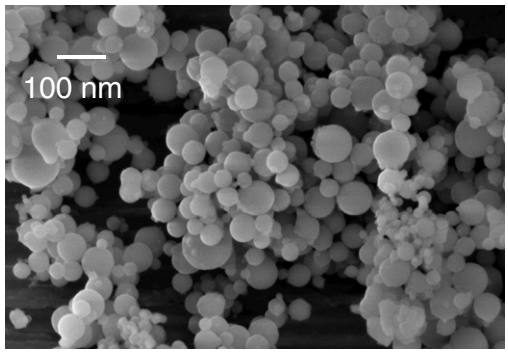

Fig. 3. High-resolution SEM micrograph of 80 nm spherical aluminum particles (courtesy of Mr. Ed. Roemer).

Figure 4 shows images of the mixture consistency at equivalence ratios of 0.5 and 1.0 for the 38 nm diameter particles. When specific surface area is high (e.g., small diameter particles) or the mixture composition is fuel-rich, the mixture behaved like a damp powder. In contrast, larger particles or fuel-lean conditions led to a highly viscous paste. Paste-like consistency yielded the highest packing densities around 1.478 g/cm^3 at $\phi = 0.67$.

Table 1
Characteristics of aluminum particles

Particle diameter (nm)	Oxide layer thickness (nm)	Active aluminum content (%)	Particle density[c] (g/cm^3)	Surface area (m^2/g)
38[a]	3.1	54.3	3.205	54.1
50[b]	2.1	68.0	3.008	41.2
80[b]	1.6	84.0	—	25.8
80[b]	1.9	81.0	3.076	26.5
80[b]	2.7	74.0	—	26.1
130[b]	2.2	84.0	—	16.5

[a] Manufactured by Technanogy, LLC.
[b] Manufactured by Nanotechnologies.
[c] Measured using a pycnometer.

Table 2
Packing densities as function of equivalence ratio and stoichiometry

Equivalence ratio	Particle diameter (nm)	Packing density (g/cm^3)
0.50	38[a]	1.384 ± 0.030
0.67	38[a]	1.478 ± 0.030
0.75	38[a]	1.055 ± 0.018
1.00	38[a]	0.726 ± 0.028
1.25	38[a]	0.731 ± 0.016
1.00	50[b]	1.395
1.00	80[b]	1.331 ± 0.106
1.00	130[b]	1.351 ± 0.020

[a] Manufactured by Technanogy, LLC.
[b] Manufactured by Nanotechnologies.

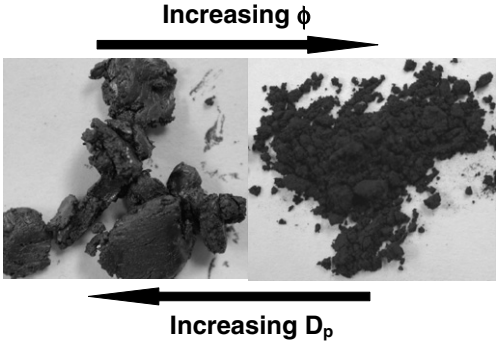

Fig. 4. Captured images of nAl–H_2O mixtures as a function of particle diameter (D_p) and equivalence ratio (ϕ).

For each test, the quartz tube was packed with the nAl–H_2O mixture and installed in the pressure vessel. The instantaneous pressure was monitored using a Setra 206 pressure transducer. Ignition was obtained by the small 1/8 in. thick propellant booster (mounted at the top of the quartz tube) initiated by a resistance-heated nichrome wire threaded through the booster. A data acquisition board was used to record the pressure transducer output at a sampling rate of 1000 Hz. The position and time of the regressing luminous front were tracked and recorded using the video record. From these data, the burning rate was determined using a curve fit to position vs. time [22].

3. Results and discussion

The burning rates as a function of pressure (0.1–4.3 MPa), overall mixture equivalence ratio (0.5–1.25), nominal particle size (38–130 nm), and particle oxide-layer thickness (1.6–2.7 nm for 80 nm particle diameter) for nano-sized aluminum particles were obtained.

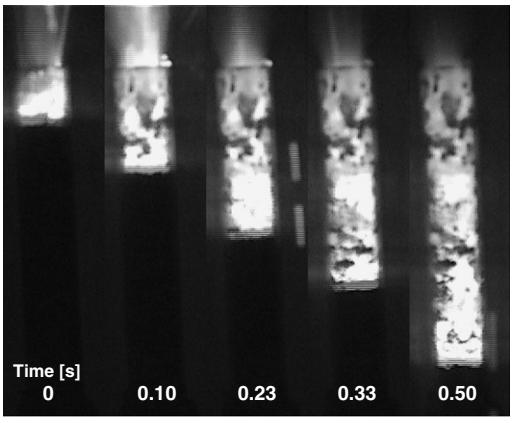

Fig. 5. Captured images of a stoichiometric 38-nm diameter nAl–H_2O mixture combusting at 3.65 MPa.

Figure 5 presents a series of video images demonstrating the normal deflagration of a stoichiometric 38-nm nAl–H_2O mixture at 3.65 MPa. The onset of ignition is represented by $t = 0$ s. After approximately 0.10 s, normal deflagration was observed and the flame steadily propagated downward until the reactants were consumed. A visible flame appeared attached to the burning surface indicating ignition at or near the surface. Depending upon the burning rate, a significant fraction of the alumina remained in the tube. The intense luminosity shown in Fig. 5 indicates the emission from the hot alumina above the propagation front. Figure 6 shows typical examples of trajectory curves (x vs. t plots), obtained from such images as those in Fig. 5. As seen in the figure, the data produced highly linear curves of x vs. t, and hence steady-state burning rates were achieved. The steadiness is also an indication of the uniformity in the packing density throughout the quartz tube.

Figure 7 shows the measured burning rates as a function of pressure for stoichiometric 38-nm diameter nAl–water mixtures. For comparison,

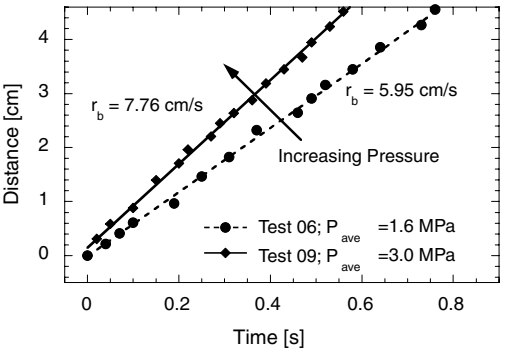

Fig. 6. Trajectory plot of two typical tests with increasing pressure.

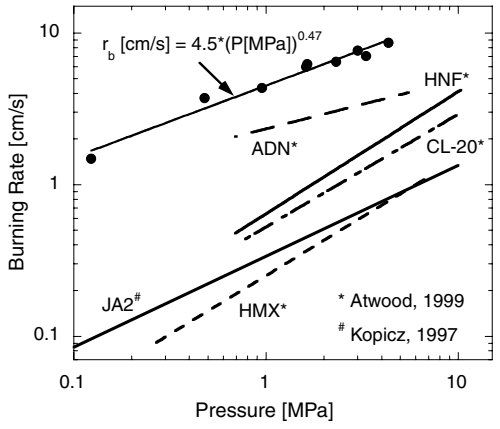

Fig. 7. Effect of pressure on burning rate for a stoichiometric 38-nm diameter nAl–H_2O mixture.

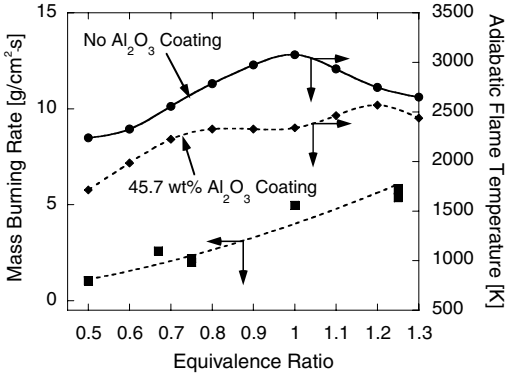

Fig. 8. Mass-burning rate per unit area and adiabatic flame temperature as a function of equivalence ratio for 38-nm diameter nAl–H_2O at $P = 3.65$ MPa.

the burning rates reported by Atwood et al. [23] and Kopicz [24] for ammonium dinitramide (ADN), hydrazinium nitroformate (HNF), cyclotetramethylene tetranitramine (HMX), hexanitrohexaazaisowurtzitane (CL-20), and JA2 (a modified double base gun propellant) are superimposed on the plot. The nAl–water burning rate is consistently higher than the other energetic materials over the pressure range studied, while having the second lowest pressure exponent. Recent closed bomb experiments with stoichiometric mixtures reveal that the combustion efficiency ranges from 87% to 94% under the conditions tested [25].

The pressure exponent of 0.47 in the burning-rate formula [24] suggests an overall first-order chemical reaction process. The phenomenon can be attributed to the collision of the water molecules on the particle surface (or another surface reaction), consistent with the adiabatic flame temperature being below the aluminum vaporization temperature (see Fig. 1). According to Wang et al. [26], for thermite reactions, where the products are predominately condensed-phase, the combustion is independent of ambient pressure when beyond 1 atm. In the present experiment, the reaction products contain significant amounts of Al_2O_3, which can cause the pressure exponent to be lower than that of a mixture with purely gas-phase products.

The influence of the overall mixture equivalence ratio was examined for the 38-nm diameter nAl at a constant pressure of 3.65 MPa (Fig. 8). As noted earlier, the overall mixture equivalence ratio affects packing density. Therefore, the mass-burning rate per unit area ($\dot{m}''_b = \rho \cdot r_b$) was employed to characterize the flame propagation behavior instead of linear burning rate because of its weak sensitivity to density. The mass-burning rate per unit area was observed to increase from $\sim$1.0 to 5.8 g/cm^2 s as the equivalence ratio increased from 0.5 to 1.25. For the two leanest mixtures, the oxide products appeared to have powder-like structure, whereas for all of the other mixtures, the products clearly had melted and formed a continuous, although porous product.

Figure 8 also includes the adiabatic flame temperatures calculated with the NASA Chemical Equilibrium Applications Program (CEA) [27]. Two calculations were performed; one without an initial oxide passivation layer and a second with a 3.1-nm thick oxide layer (equivalent to 45.7 wt% of the total particle mass). For the case without the oxide coating, the temperature increases with increasing equivalence ratio, and only exceeds the Al vaporization temperature near the stoichiometric mixture ratio. A further increase in the ϕ then reduces the flame temperature. For the case with the oxide included in the initial mixture, the adiabatic flame temperature never exceeds the Al vaporization temperature, even at the stoichiometric mixture ratio. In fact, stoichiometric and slightly lean conditions, the flame temperature is limited by the melting temperature of the oxide layer. Since these calculations are based upon the overall mixture equivalence ratio, local temperatures could be higher if the particles burn in a diffusion-controlled manner. However, the pressure sensitivity results appear to suggest that the combustion is kinetic controlled. Consequently, high transport rates could be expected to lower the local temperature closer to the bulk mixture values. Thus, for fuel-lean conditions, the burning-rate behavior is consistent with the increase in the flame temperature with increasing ϕ. The lower flame temperature for fuel-lean mixtures reduces the reaction rate and hence the heat feedback to the surface. For fuel-rich mixtures, the burning rate is expected to plateau and eventually decrease. The peak on the fuel-rich side results from the product gas

composition becoming nearly pure hydrogen, as opposed to a H_2/H_2O mixture.

The effect of pressure was also studied for lean mixtures. Figure 9 presents the burning rate as a function of pressure for an equivalence ratio of 0.67. Results indicate that the excess water does not influence the overall reaction order (as reflected by the pressure exponent), although as discussed above the burning rates are lower due to the lower mixture temperatures. Ivanov [18] also obtained measurements for the same equivalence ratios and found that excess water significantly affected the pressure exponent, nearly doubling it, compared to their stoichiometric value. Their data, however, cannot be directly compared to the present results since a gelling agent was included in the mixture in their experiments, larger aluminum particles were used, and packing densities were not reported. Furthermore, Ivanov et al. [18] also noted the burning rate (~1.5 cm/s at ~7 MPa) at $\phi = 0.67$ (40% by mass) was higher than that at the stoichiometric condition. These trends are opposite to the results reported in the present study. Ivanov et al. [18] also observed the existence of a foamy layer which occurred between the boiling temperature of water and ~540–570 K. In our experiments, such formation of a foamy layer was not observed, possibly because no gelling agent was introduced in the nAl–H_2O mixtures.

Burning rates were also obtained as a function of aluminum particle diameter. Four different diameters were investigated: 50 nm, 80 nm, 130 nm, and 5 μm. Ignition of the 5-μm aluminum particles was not achieved for the pressures and type of ignition system used in this study. These results were anticipated since the specific surface area of micronized particles is relatively small, and thus, the mixture is less gelled. In addition, the rate of energy delivery from the igniter was not rapid enough to heat up the micron-sized aluminum to its ignition temperature, and consequently, much of the energy from the igniter was expended to vaporize the water without reacting with the aluminum. Another contributing factor is that micron-sized aluminum particles need much higher temperatures (~2000 K) than nAl (~900 K) to ignite [13,14] even though having larger active aluminum content. In contrast, nAl particles have the ability to absorb large amounts of water on the surface (thus gelling and improving the mixedness of the mixture) as well as to heat up quicker (smaller heat capacity). Figure 10 shows the burning rates of nAl–H_2O mixtures as a function of particle diameter. Decreasing the particle size from 130 to 50 nm resulted in a 2.57 times increase in burning rate. A linear relationship of the burning rate with respect to particle diameter was obtained, indicating the prevalence of a diffusion-controlled process. These results appear contradictory to the pressure dependency of the burning rate presented earlier, which indicate an overall first-order reaction. For energetic composite self-propagating high-temperature synthesis (SHS), Tomasi and Munir [28] note that the influence of particle size on burning rate has been shown to have a D^{-1} dependence for diffusion-controlled reaction kinetics, but the relationship $D^{-0.5}$ proposed when the kinetics are controlled by surface reactions has yet to be demonstrated. In the present system, both transport and chemistry could affect the burning behavior, leading to the D^{-1} correlation and a strong pressure dependence. For example, because of the distribution in particle size, a fraction of the particles could be kinetically dominated and not diffusion dominated, which would be analogous to ammonium perchlorate composite propellants that have both pressure and particle size dependencies. Another possibility is that the particles are heated and then dynamically explode by thermal stresses, whereas the heating process is diameter dependent. The resultant fine droplets would be kinetically controlled. In any case, these

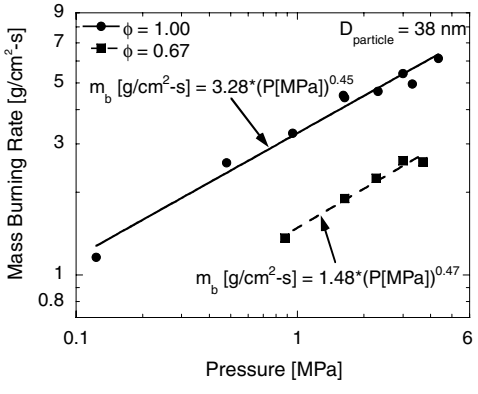

Fig. 9. Effect of equivalence ratio on mass-burning rate per unit area as a function of pressure.

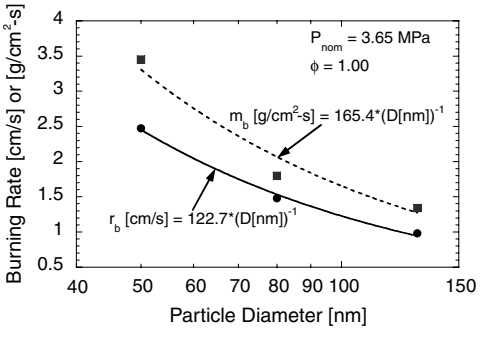

Fig. 10. Burning rate as a function of aluminum particle diameter.

observations are very unusual and defy simple global arguments.

The effect of oxide layer thickness was also investigated for stoichiometric mixtures of nAl and liquid water at a nominal pressure of 3.65 MPa. For the limited range of oxide tested, the oxide thickness did not appear to have a strong influence on the linear and mass-burning rates. It is believed that depending on the heating rate and the thickness of the oxide layer, high pressure can build inside the oxide shell and promote mini particle explosions [29]. Under the current test conditions, mini particle explosions were not directly observed, but this may be difficult to observe due to the challenges in implementing diagnostic techniques at such small scales.

4. Conclusions

The combustion of nano-aluminum (nAl) and liquid water was characterized without the use of any gelling agent for a broad range of pressure, mixture composition, and particle size. The effect of oxide layer thickness was also considered. The major conclusions of this work are as follows:

1. Quasi-homogeneous mixtures of nAl and liquid water were successfully ignited and results on linear burning rate and mass-burning rate per unit area appear to be the first reported.
2. A burning-rate pressure exponent of 0.47 was obtained and found to be independent of excess water content in the mixtures.
3. The burning rate depends strongly on the ϕ due to its influence on the adiabatic flame temperature and modifications of the mixture properties. Under most of the conditions, the flame temperature is expected to be below the Al vaporization temperature and close to the melting temperature of the oxide. Consequently, combustion occurred heterogeneously at the particle surfaces, making the high burning rates achieved in this study all the more interesting.
4. At $P = 4.3$ MPa, the linear burning rate was found to be 8.6 ± 0.4 cm/s, which corresponds to a mass-burning rate per unit area of 6.1 g/cm^2 s. These rates are extremely fast surpassing several highly energetic propellants.
5. The mass-burning rates per unit area were found to be inversely proportional with respect to particle diameter (D^{-1}), demonstrating a 2.57 times increase when the particle diameter was decreased from 130 to 50 nm.

Future research will specifically examine, in detail, the efficiency of the reaction through calorimetry-type experiments where the heat release, pressure rise, and amount of gas-phase hydrogen will be used to quantify the efficiency.

Acknowledgments

This work was sponsored by the U.S. Army Research Office under the Multi-University Research Initiative under Contract No. W911NF-04-1-0178 and the Office of Naval Research (ONR) under Grant No. N00014-03-1-0595. The support and encouragement provided by Drs. David Mann, Kevin L. McNesby, and Gabriel Roy are gratefully acknowledged. S.F.S. and B.C.T. are supported by the Joint Munitions Program (DoD/DOE) at the Los Alamos National Laboratory (LANL), which is operated by the University of California for the U.S. Department of Energy under the Contract No. W-7405-ENG-36. The authors thank personnel at LANL, specifically Mr. Ed Roemer for the SEM micrographs of the particles, Mr. Eric Sanders for supplying the 38-nm aluminum particles, and Dr. Joseph T. Mang for SAS and BET data for the 80-nm particles.

Appendix A. Supplementary data

Supplementary data associated with this article can be found in the online version at doi:10. 1016/j.proci.2006.08.056.

References

[1] M.W. Beckstead, *Combustion, Explosion, and Shock Waves* 41 (5) (2005) 533–546.
[2] K.P. Brooks, M.W. Beckstead, *Journal of Propulsion and Power* 11 (4) (1995) 769–780.
[3] W.M. Lee, Report No. AD-A269223, Naval Surface Warfare Center, 1993.
[4] T.F. Miller, J.D. Herr, AIAA 2004–4037, 2004.
[5] A. Ingenito, C. Bruno, *Journal of Propulsion and Power* 20 (6) (2004) 1056–1063.
[6] W.C. Tao, A.M. Frank, R.E. Clements, J.E. Shepherd, *Aluminum Metal Combustion in Water by High Speed Microphotography*, International Symposium on Optical and Optoelectronic Applied Science and Engineering Exhibit, vol. 1346, 1990.
[7] P. Bucher, R.A. Yetter, F.L. Dryer, T.P. Parr, D.M. Hanson-Parr, *Proc. Combust. Inst.* 27 (1998) 2421–2429.
[8] I. Glassman, *Combustion*, third ed., Academic Press, Orlando, 1996 (Chapter 9).
[9] F.A. Williams, *Combustion Theory*, Addison Wesley Co., Redwood City, CA, 1985.
[10] F.A. Williams, in: F.L. Dryer, R.F. Sawyer (Eds.), *Some Aspects of Metal Particle Combustion*, Gordon and Breach, The Netherlands, 1997, p. 267.
[11] R.A. Yetter, F.L. Dryer, in: H. Ross (Ed.), *Metal Particle Combustion and Classification*, Academic Press, 2001 (Chapter 6).
[12] L.F. Ernst, F.L. Dryer, R.A. Yetter, 37th Combustion/25th Airbreathing Propulsion/19th Propulsion Systems Hazards/ and 1st Modeling and Simulation JANNAF Subcommittees Joint Meeting, 2000.

[13] T. Parr, C. Johnson, D. Hanson-Parr, K. Higa, K. Wilson, JANNAF Combustion Subcommittee, 2003.
[14] M.A. Trunov, M. Schoenitz, E.L. Dreizin, *Propellants, Explosives, and Pyrotechnics* 30 (1) (2005) 36–43.
[15] T.P. Parr, D.M. Hanson-Parr, R.A. Yetter, 36th JANNAF Combustion Subcommittee, 1999.
[16] K. Park, D. Lee, A. Rai, D. Mukherjee, M.R. Zachariah, *Journal of Physical Chemistry B* 109 (15) (2005) 7290–7299.
[17] V.G. Ivanov et al., *Combustion, Explosion, and Shock Waves* 30 (4) (1994) 569–570.
[18] V.G. Ivanov et al., *Combustion Explosion and Shock Waves* 36 (2) (2000) 213–219.
[19] M.L. Pantoya, S.F. Son, W.C. Danen, B.S. Jorgensen, B.W. Asay, J.R. Busse, J.T. Mang, in: A.M. Miziolek, S.P. Karna, L.M. Mauro, R.A. Vaia (Eds.), *Characterization of Metastable Intermolecular Composites*, Oxford University Press, NC, American Chemical Society, 2005, pp. 227–899.
[20] B.S. Bockmon, M.L. Pantoya, S.F. Son, B.W. Asay, J.T. Mang, *Journal of Applied Physics* 98 (6) (2005) 64903–64910.
[21] B.W. Asay, S.F. Son, J.R. Busse, J.M. Oschwald, *Propellants, Explosives, and Pyrotechnics* 29 (4) (2004) 216–219.
[22] G.A. Risha, A. Ulas, K.K. Kuo, D.E. Koch, C.P. Ludwig, R. Glick, AIAA Paper No. 99–2632, 1999.
[23] A.I. Atwood, T.L. Boggs, P.O. Curran, T.P. Parr, D.M. Hanson-Parr, *Journal of Propulsion and Power* 15 (6) (1995) 747.
[24] C.F. Kopicz, *Combustion Behavior and Thermo-Chemical Properties of JA2 Propellant*, The Pennsylvania State University, 1995.
[25] G.A. Risha, S.F. Son, B.C. Tappan, V. Yang, R.A. Yetter, Combustion and Conversion Efficiency of Nanoaluminum–Water Mixtures, 33rd International Pyrotechnics Seminar, 2006.
[26] L.L. Wang, Z.A. Munir, M. Maximov, *Journal of Materials Science* 28 (1993) 3693–3708.
[27] B.J. Mcbride, S. Gordon, Reference Publication 1311, NASA, 1996.
[28] R. Tomasi, Z.A. Munir, *Journal of American Ceramics Society* 82 (8) (1999) 1985–1992.
[29] S. Wang, Y. Yang, H. Yu, D.D. Dlott, *Propellants, Explosives, and Pyrotechnics* 30 (2) (2005) 148–155.

Comment

Richard Axelbaum, Washington University, USA. What was the size distribution of the 38 nm particles? Were they size-selected, or as-produced?

Reply. The nano-aluminum used is this study was obtained from Technanogy, LLC. The material was not specified. In fact, the aluminum is their typical 38 nm particles. They mass produce three general sizes; 38, 80, and 120 nm. Mang et al. [1] performed extensive analyses on similar materials from the same manufacturer. Their results show for particles identified as 38 nm in diameter, the size distribution ranged from 30 to 44 nm.

Reference

[1] J.T. Mang, R.P. Hjelm, S.F. Son, P.D. Peterson, B.S. Jorgensen, Characterization of components of nano-energetics by small-angle scattering techniques, *Journal of Materials*, Los Alamos National Laboratory, Report #LA-UR-06-3251, Los Alamos, NM, 2006.